

EVOLUTION OF THE NEAR-INFRARED TULLY-FISHER RELATION: CONSTRAINTS ON THE RELATIONSHIP BETWEEN THE STELLAR AND TOTAL MASSES OF DISK GALAXIES SINCE $Z \sim 1$

CHRISTOPHER J. CONSELICE^{1,2}, KEVIN BUNDY¹, RICHARD S. ELLIS¹, JARLE BRICHMANN^{3,4},

NICOLE P. VOGT⁵, ANDREW C. PHILLIPS⁶

Accepted to the Astrophysical Journal

ABSTRACT

Using a combination of Keck spectroscopy and near-infrared imaging, we investigate the K-band and stellar mass Tully-Fisher relation for 101 disk galaxies at $0.2 < z < 1.2$, with the goal of placing the first observational constraints on the assembly history of halo and stellar mass. Our main result is a lack of evolution in either the K-band or stellar mass Tully-Fisher relation from $z = 0 - 1.2$. Furthermore, although our sample is not statistically complete, we consider it suitable for an initial investigation of how the fraction of total mass that has condensed into stars is distributed with both redshift and total halo mass. We calculate stellar masses from optical and near-infrared photometry and total masses from maximum rotational velocities and disk scale lengths, utilizing a range of model relationships derived analytically and from simulations. We find that the stellar/total mass distribution and stellar-mass Tully-Fisher relation for $z > 0.7$ disks is similar to that at lower redshift, suggesting that baryonic mass is accreted by disks along with dark matter at $z < 1$, and that disk galaxy formation at $z < 1$ is hierarchical in nature. We briefly discuss the evolutionary trends expected in conventional structure formation models and the implications of extending such a study to much larger samples.

1. INTRODUCTION

In the currently popular hierarchical picture of structure formation, galaxies are thought to be embedded in massive dark halos. These halos grow from density fluctuations in the early universe and initially contain baryons in a hot gaseous phase. This gas subsequently cools and some fraction eventually condenses into stars. Much progress has been made in observationally delineating the global star formation history and the resulting build-up of stellar mass (e.g., Madau et al. 1998, Brinchmann & Ellis 2000; Dickinson et al. 2003; Bundy, Ellis & Conselice 2005). However, many of the physical details, particularly the roles played by feedback and cooling, essential for a full understanding of how galaxies form, remain uncertain. Models (e.g., van den Bosch 2002; Abadi et al. 2003) have great predictive power in this area but only by assuming presently-untested prescriptions for these effects. Obtaining further insight into how such processes operate is thus an important next step not only in understanding galaxy evolution, but also in verifying the utility of popular models, as well as the hierarchical concept itself. One approach towards understanding this issue is to trace how the stellar mass in galaxies forms in tandem, or otherwise, with its dark mass.

The first step in this direction began with studies of scaling relations between the measurable properties of disk galaxies, specifically the relation between luminosity and maximum rotational velocity (Tully & Fisher 1977). Studies utilizing roughly a thousand spiral galaxies have

revealed a tight correlation between absolute magnitude and the maximum rotational velocity for nearby galaxies (Haynes et al. 1999). The limited data at high redshift suggests the TF relation evolves only modestly, equivalent to at most 0.4 - 1 magnitudes of luminosity evolution to $z \sim 1$ (Vogt et al. 1997; Ziegler et al. 2002; Bohm et al. 2004). How the Tully-Fisher relation evolves with redshift is still controversial, although it appears that fainter disks evolve the most (Bohm et al. 2004), and that selection effects are likely dominating the differences found between various studies. Furthermore, it has been difficult for modelers to reproduce the Tully-Fisher relation to within 30% (e.g., Cole et al. 2000), making it an important constraint on our understanding of the physics behind galaxy formation.

Unfortunately, any interpretation of the TF relation is complicated by the fact that both luminosity and virial mass might be evolving together. A more physically-motivated comparison would be between stellar and virial mass. Not only does this relation break potential degeneracies in the TF technique, but it also samples more fundamental quantities. In this paper we begin this task by investigating the evolution in the fraction of the total mass that is in a stellar form. This can be accomplished with some uncertainty by contrasting the *stellar mass* of a galaxy with its *halo mass*. We selected disk galaxies for our initial study since these two quantities can be effectively probed observationally for these galaxies with various assumptions (e.g., van den Bosch 2002; Baugh et al. 2005).

This paper presents the first study of the near-IR TF

¹ California Institute of Technology, Mail Code 105-24, Pasadena CA 91125

² NSF Astronomy & Astrophysics Postdoctoral Fellow

³ Max-Planck-Institut für Astrophysik, Karl-Schwarzschild-Str. 1, 85740 Garching bei München

⁴ Centro de Astrofísica da Universidade do Porto, Rua das Estrelas - 4150-762 Porto, Portugal

⁵ New Mexico State University, Astronomy Department, Las Cruces, NM 88003

⁶ Lick Observatory, University of California, Santa Cruz, CA 95064

relation, as well as a comparison between stellar and halo masses, for 101 disk galaxies within the redshift range $0.2 < z < 1.2$ drawn mostly from the DEEP1 redshift survey (Vogt et al. 2005). Our goal is to address several questions relating to the mass assembly history of disks. As our sample is not formally complete in any sense, we cannot derive general conclusions concerning the history of *all* present-day disks. However, we can determine whether the disks selected from the DEEP1 survey in the sampled redshift range are still accreting matter and converting baryons into stellar disks at a significant rate. We construct stellar mass Tully-Fisher and stellar mass/halo mass relation for our sample and find that there is little evolution in either from $z \sim 0-1.2$. This suggests that the dark and stellar components of disk galaxies grow together during this time.

The paper is organized as follows: §2 contains a description of the sample including the fields used and the different data products and a discussion on quality control. §3 describes how various quantities, such as the halo and stellar masses, are derived from the basic data. §4 presents our results and §5 summarizes our conclusions. We assume the following cosmology throughout this paper: $H_0 = 70 \text{ km s}^{-1} \text{ Mpc}^{-1}$, $\Omega_\Lambda = 0.7$ and $\Omega_m = 0.3$.

2. DATA

2.1. The DEEP1 Extended Sample

Our sample consists of 101 galaxies, 93 of which are drawn from the DEEP1 survey (see Vogt et al. 2004; Simard et al. 2002; Weiner et al. 2004), and 8 of which were obtained independently. Each of these systems has a resolved rotation curve which was obtained with the Keck telescope using LRIS (Oke et al. 1995) in the redshift range $z \sim 0.2$ to $z \sim 1.2$. The additional data presented in this paper, which enables stellar masses to be compared with virial masses, consists of near-infrared imaging described in §2.2.

Full details of the selection criteria for the galaxies are discussed in DEEP1 papers (Vogt et al. 1996, 1997, 2005) to which the interested reader is referred. Moreover, the necessary assumptions implicit in the derivation are detailed in those papers, to which we refer the reader. Briefly, galaxies were selected morphologically as elongated disks in Hubble Space Telescope (HST) F814W (I_{814}) images with $I_{814} < 23$. The inferred inclination was chosen to be greater than 30° to facilitate a measurement of the rotational velocity. The optical images used for both photometric and morphological analyses come from HST Wide Field Planetary Camera-2 (WFPC2) observations of the Groth Strip (Groth et al. 1994; Vogt et al. 2004), the Hubble Deep Field (Williams et al. 1996), and CFRS fields (Brinchmann et al. 1998). Using I_{814} images, structural parameters were determined for each galaxy using the GIM2D and GALFIT packages (Simard et al. 2002; Peng et al. 2002). We fit a two-component model to the surface brightness distribution, assuming a de Vaucouleurs law for the bulge, and an exponential for the disk component. Based on these fits, the disk scale length, R_d , and bulge-to-disk ratio (B/D) were determined. The uncertainties in the R_d values determined through this method are possibly underestimated, as has been explored through careful 2-D fitting (e.g. Jong et al 1996). To be inclusive

of possible effects, we will incorporate an additional 30% uncertainty for our overall error on the measured values of R_d .

Details of the observations, reductions and extraction of maximal rotational velocities V_{\max} from the LRIS spectroscopy are presented in Vogt et al. (1996, 1997, 2005). Briefly, each disk galaxy was observed along its major axis, as determined from the HST images (Simard et al. 2002). The maximum velocity, V_{\max} , is determined by fitting a fixed form for the rotation curve scaled according to the I_{814} disk scale length R_d . The assumed rotation curve has a linear form which rises to a maximum at $1.5 \times R_d$, and remains flat at larger radii. Our assumption that $1.5 \times R_d$ is the radius where the rotation curves for disks reach their maximum is reasonable, based on a similar behavior for local disk systems of similar magnitudes (Persic & Salucci 1991; Sofue & Rubin 2001). Our rotation curves are also visible out to several scale lengths, or roughly $2-5''$ (e.g., Vogt et al. 1997), adequate for measuring V_{\max} . This model form is then convolved with a seeing profile that simulates the conditions under which the observations were taken, and V_{\max} is determined by iterative fitting. Effects from the width of the slit, slit misalignment with the major axis, and varying inclination were taken into account when performing these fits, and calculating the resulting errors. Typically, V_{\max} is determined to a precision of 10-20% due to these various sources (e.g., Vogt et al. 1997).

2.2. Near-Infrared Imaging

The new data we present in this paper consist of deep near-infrared observations of the DEEP1 extended sample. Precision near-infrared photometry is the critical ingredient for determining stellar masses for our sample (Brinchmann & Ellis 2000). Photometry was acquired with a K_s filter with three different instruments: the Keck Near Infrared Camera (NIRC, Matthews & Soifer 1994), the UKIRT Fast-Track Imager (UFTI, Roche et al. 2003), and the Cooled Infrared Spectrograph and Camera for OHS (CISCO, Motohara et al. 2002) on the Subaru 8.4 meter telescope (see Bundy et al. 2004 for a more detailed description of these data). NIRC has a field of view of $38''$ and a pixel scale of $0.15'' \text{ pixel}^{-1}$. The equivalent numbers for UFTI are: $96''$ field of view, with a pixel scale of $0.091'' \text{ pixel}^{-1}$. The CISCO camera has a field of view of $108''$ with a pixel scale of $0.105'' \text{ pixel}^{-1}$. The typical depths for these images is $K_s = 20.5-21$ (Vega) with a typical seeing of $\sim 0.8''$.

In each case, the infrared data were taken with a dither pattern whose step size exceeded the typical size of the galaxies of interest. The data were reduced by creating sky and flat-field images from sets of disregistered neighboring science frames. Standard stars were observed for calibration purposes during the observations. Some images taken in good seeing but through thin cloud were subsequently calibrated in photometric conditions via shallower exposures taken with the Wide Field Infrared Camera (WIRC, Wilson et al. 2003) on the Hale 5 meter telescope.

2.3. Rest-Frame Quantities

We measure our photometry in the K_s -band, and HST I_{814} and V_{606} bands, within a scale-length factor, either

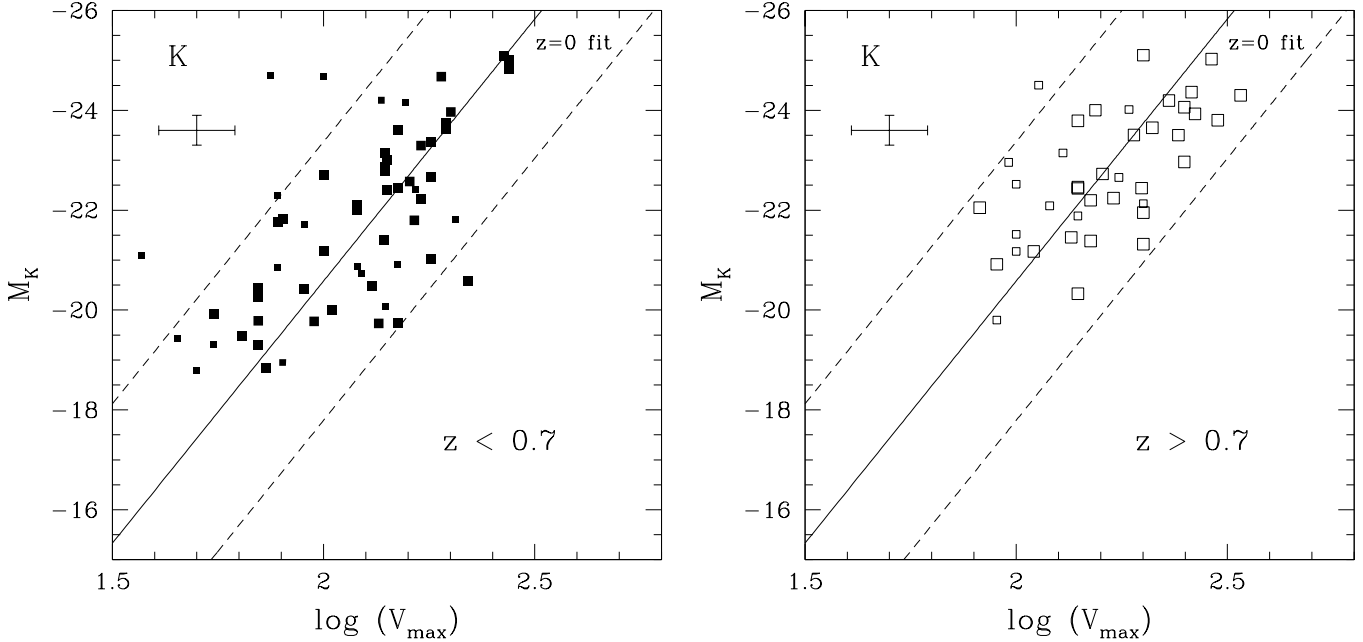


FIG. 1.— The rest-frame K-band Tully-Fisher relation for our sample of disks. The panels are divided into different redshift bins, higher and lower than $z = 0.7$. The solid and dashed lines is the $z \sim 0$ Tully-Fisher relation found by Verheijen (2001) and its $\pm 3\sigma$ scatter. The average error is also plotted in each panel. The large points have errors lower than this average, while smaller points have errors larger than the average.

1.5R_d or 3R_d, both of which are generally large enough to avoid seeing effects from the K_s imaging. We then extrapolate the total magnitudes, within each band, out to infinite radius by using the fitted parameters for an exponential disk derived in the HST I₈₁₄ band. To compare observables over a range in redshift, it is necessary to reduce all measures to a standard rest-frame. Galactic extinction corrections were applied using the formalism of Schlegel, Finkbeiner & Davis (1998) and internal extinction was accounted for according to measured inclinations and luminosities using the precepts of Tully et al. (1998). It is debatable whether internal extinction corrections derived for nearby spirals are applicable to higher redshift disks. Our sample is mostly composed of systems with M_B > -22 where extinction could be a cause for concern. However, direct extinction measurements in moderate redshift disks, determined through overlapping pairs, find a modest overall extinction (White, Keel & Conselice 2000).

To derive absolute magnitudes and rest-frame colors, we estimated non-evolutionary k -corrections. The K-band k -corrections were computed from spectral energy distributions determined alongside the stellar mass fits. We experimented with both the original algorithm developed by Brinchmann & Ellis (2000) and also an independent one developed by Bundy, Ellis & Conselice (2005, see §3.2). Both methods agree very well. The approach is similar to that used by Vogt et al. (1996, 1997) where k -corrections were calculated from model SEDs from Gronwall & Koo (1995) based on various star formation histories in the Bruzual & Charlot (1993) code. We also note that our derived k -correction values are very similar to non-evolutionary k -corrections derived by Poggianti

(1997) using SEDs from Poggianti & Barbaro (1996).

3. MASS ESTIMATORS

3.1. Virial and Halo Masses

The virial mass of a galaxy - that is, the combined total of the dark, stellar and gaseous components - is perhaps its most fundamental property. However, obtaining an accurate estimate from observed quantities is necessarily difficult since there is no *a priori* agreed model for the relative distributions of the various components. Our approach to this challenge will be to use both analytical techniques and semi-analytical simulations to investigate the relationship between the total halo mass and our dynamical and structural observables. Although necessarily approximate and debatable in terms of the assumptions made, we will attempt, where possible, to investigate the uncertainties involved by contrasting the two approaches in the context of our data.

For a simple virialized system, such as a circularly rotating disk, we can place constraints on the total mass within a given radius R independent of model assumptions. If $R > 1.5 \times R_d$, where we estimate the maximum rotational velocity V_{max} is reached, the mass within R is given by,

$$M_{\text{vir}}(< R) = V_{\text{max}}^2 R / G, \quad (1)$$

where $R > 1.5 \times R_d$. This assumes that the rotation curve reaches the maximum velocity by $1.5 \times R_d$, (Persic & Salucci 1991), otherwise V_{max} should be replaced by V(R).

There are a few possible approaches for determining total halo masses, some of which require the use of simulations to convert observed dynamical qualities, usually V_{max}, into halo masses. We take a basic approach using

eq. (1) to obtain the total mass with a given radius, and take a suitably large total radius of 100 kpc to measure the total halo mass. This is often the extent of disk HI rotation curves, and similar to the sizes of dark matter halos (e.g., Sofue & Rubin 2001). Another approach now being used (e.g., Bohm et al. 2004) has been proposed by van den Bosch (2002). In this case, it is argued from analytic simulations of disk galaxy formation that the quantity $M_{\text{vdB}} = 10.9 \times M_{\text{vir}}(R_d)$ gives, on average, the best empirical representation of the virial mass for simulated disks. The zero-point of the relationship between $R_d V_{\text{max}}^2/G$ and virial mass is claimed to be independent of feedback and independent of the mass of the halo (van den Bosch 2002).

Semi-analytic models based on Λ CDM (e.g., Cole et al. 2000; Benson et al. 2002; Baugh et al. 2005) suggest, however, that the ratio between $V_{\text{max}}^2 R_d/G$ and halo mass is not as simple as the above formalism implies. The latest *Galform* models from Baugh et al. (2005) and Lacey (priv. communication) show that equation [1] and van den Bosch (2002) under-predicts the dark halo mass. These models show that the relationship between the virial mass at R_d and the total halo mass changes as a function of mass in the sense that the ratio is higher for lower mass halos. Physically this can be understood if high mass halos have a larger fraction of their baryonic mass in a hot gaseous phase that is not traced by the formed stellar mass. Using the *Galform* models to convert our observables into a total halo mass is however potentially inaccurate as these models cannot reproduce the Tully-Fisher relation to better than 30%. However, there are reasons to believe that the semi-analytic models put the correct amount of halo mass into their modeled galaxies (e.g., Benson et al. 2000). This however does not necessarily imply that the V_{max} values in these models are able to accurately match the halo masses. Independent determinations of total halo masses are necessary to perform this test. However, the masses from this approach match within 0.5 dex the masses from using eq. (1) with a suitably large total radius.

With these caveats in mind, we have used the *Galform* model results to fit the relationship between the virial mass at R_d (eq. 1), and the total mass of the halo (M_{halo}), a ratio which we call $\mathfrak{R} = M_{\text{vir}}(R_d)/M_{\text{halo}}$. We fit \mathfrak{R} as a linear function of $M_{\text{vir}}(R_d)$, such that $\mathfrak{R} = \alpha \times \log(M_{\text{vir}}(R_d)) + \beta$. Using the *Galform* results we fit α and β at redshifts $z = 0, 0.4, 0.8, 1.2$. We find that the functional form of \mathfrak{R} does not change significantly with redshift, with typical values $\alpha = -0.1$ and $\beta = 1.3$. The value of the halo mass M_{halo} is then given by:

$$M_{\text{halo}} = M_{\text{vir}}(R_d)/\mathfrak{R}. \quad (2)$$

Observational and model uncertainties contribute to errors on these virial and halo mass estimates in two ways. Measured scale lengths given by the GIM2D and GALFIT fitting procedure (§2.1), give an average error of 0.12 kpc, although we add an extra error to this to account for systematics seen when performing one component models to disks/bulge systems (de Jong 1996). At the same time, systematic difficulties in the rotation curve analysis (§2.1) can arise. Vogt et al. (2005) discuss these issues in some detail and conclude the average error is $\sim 27 \text{ km s}^{-1}$ (typically $\simeq 10\text{--}20\%$). Following the discussion of rotation curve fitting in §2.1, it is possible we do not measure the true

V_{max} required for insertion in equations (1 & 2). Even a modest underestimate of V_{max} would lead to a significant error in M_{vir} . In combination, these measurement uncertainties imply virial and halo masses precise to no better than 30%. The semi-analytic method for computing total halo masses is likely limited, and thus we also investigate the total halo masses found through the van den Bosch (2002) formalism, and through the use of equation (1) out to 100 kpc. We find that the total halo mass through eq. (1), eq. (2) and van den Bosch (2002) are all fairly similar. We account for these differences in our use of total halo masses in §4.3.

3.2. Stellar Masses

Our procedure for deriving stellar masses follows the multi-color method introduced by Brinchmann & Ellis (2000). Combining HST V_{606} , I_{814} , and near-infrared K_s photometry for a galaxy of known redshift, we fit a range of template SEDs synthesized using software by Bruzual & Charlot (2003). Our photometry is done in a matched aperture large enough to avoid seeing problems associated with the K_s -band. These fitted SEDs constrain the K_s -band mass/light ratio. Our code for computing stellar masses only uses models with ages less than the age of the universe at the redshift observed. A χ^2 analysis normalized by the near infrared K_s -band luminosity yields the stellar mass. The template SEDs were constructed sampling a range of exponentially-declining star formation rates, metallicities and ages with a Salpeter IMF. Using other stellar mass functions, such as Chabrier, Kennicutt or Kroupa would result in computed stellar masses that are smaller by < 0.3 dex. We further assumed a simple exponentially declining star formation history with τ values ranging from 0.001 - 15.0 Gyr, and metallicities from $Z=0.005\text{--}5$ in solar units. Typical uncertainties in this method are a factor of three (Brinchmann & Ellis 2000; Papovich, Dickinson & Ferguson 2001; Drory et al. 2004; Bundy, Ellis & Conselice 2005).

The SED is constrained by the observed colors as measured in an aperture of radius $1.5 \times R_d$ in each band which is optimal in terms of signal-to-noise (S/N). We assume that there are no color gradients and use the colors measured within this aperture as the global color. The total K_s -band light is measured by extrapolating the $1.5 \times R_d$ flux to infinity, assuming the same exponential fit as measured in the HST I_{814} image.

Errors on the stellar masses arising from photometric uncertainties can be determined in a Monte Carlo fashion. Simulated exponential disks of a known magnitude were inserted into the reduced HST and ground based images and photometrically recovered using the tools that were applied to the sample. The simulated disks were arranged to randomly sample the selected ranges of disk scale-length R_d and inclination. The derived photometric errors were then input into the stellar mass calculations from which a 1σ range was calculated. The average error in M_* is 0.47 dex.

The calculation of stellar masses through this technique is limited to a degree by systematics which are difficult to constrain with the current data set, with K_s -band magnitude errors only a small source of uncertainty. The models of the spectral evolution of galaxies depend both on the

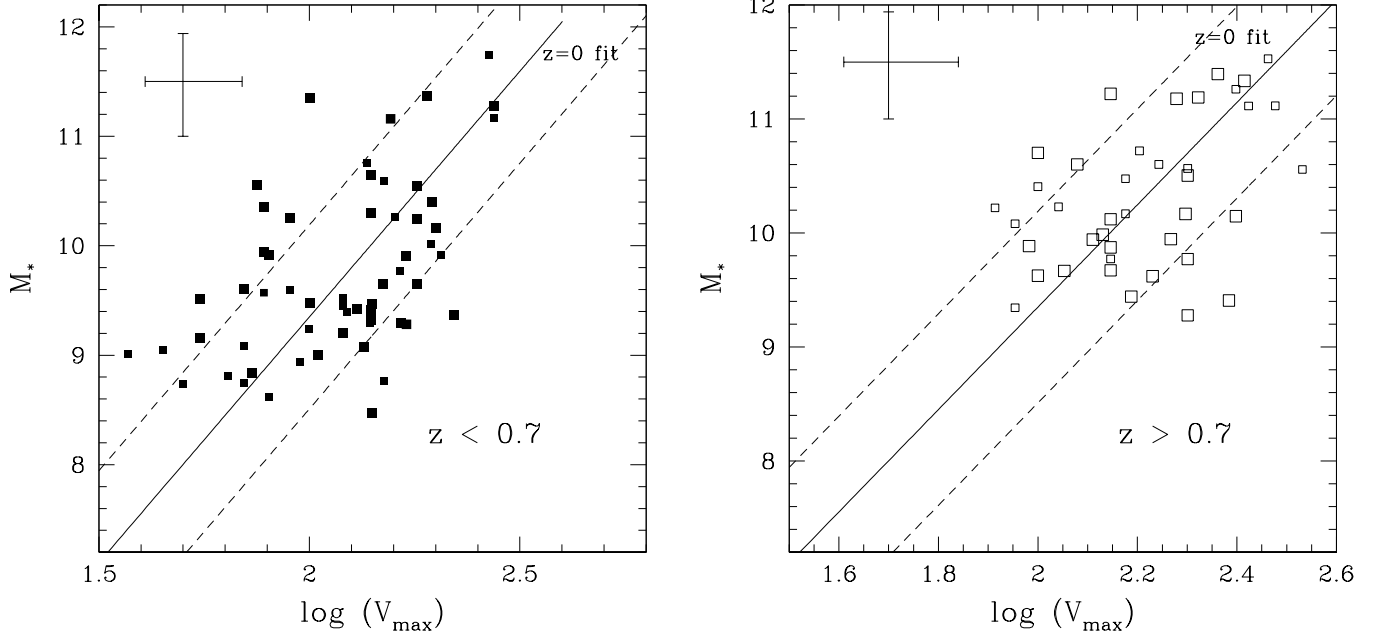


FIG. 2.— The stellar mass Tully-Fisher relation plotted as a relation between M_* and V_{\max} . The solid and dashed line is the $z = 0$ relationship found by Bell & de Jong (2001) for nearly disks and its $\pm 3\sigma$ scatter. The error bar is the average with large points having errors lower than this average, and smaller points having errors larger than the average.

observed stellar libraries and underlying theory, and some fundamental uncertainties remain (c.f. Bruzual & Charlot 2003). We expect uncertainties of about 5-10%, given the range of possible models (Charlot, Worthey & Bressan 1996). This is not important for the conclusions in this paper but might be an issue with larger and more accurate datasets in the future.

We also cannot constrain the amount of recent star formation produced in bursts (e.g., Kauffmann et al. 2003; Bell & de Jong 2001), resulting in a slight systematic overestimate of the stellar mass. The latter effect only becomes important at large burst fractions and should be $< 10\%$ for our big spirals (c.f. Drory et al 2003). The final systematic uncertainty is the dust correction adopted. We use the Calzetti (1997) extinction law in our stellar mass calculations, although other extinction laws produce very small differences (at most 10-20%) in the resulting stellar mass (Papovich et al. 2001). Taken together we are likely to have systematic uncertainties in our stellar mass estimates amounting to ~ 0.15 dex which is lower than our random uncertainty, thus they will not influence our results.

4. RESULTS

4.1. *K*-band Tully-Fisher Relation

The Tully-Fisher (TF) relation has been the traditional method for investigating how dark halos and the stellar components of disk galaxies relate. The optical relation has been studied in disks galaxies out to redshifts $z \sim 1$ by e.g., Vogt et al. (1996, 1997, 2005), Ziegler et al. (2002) and Bohm et al. (2004). These investigations have found between 0.4 and ~ 1 magnitudes of rest-frame B-band luminosity evolution in disks between $z \sim 0$ and $z > 0.5$.

This luminosity evolution is derived by assuming that the slope of the TF relation at high redshift is the same as it is at $z \sim 0$. The question of differential evolution in the relation (Ziegler et al. 2002; Bohm et al. 2004), for example that the faintest galaxies evolve more rapidly, remains an important unknown.

Although the purpose of this paper is to move beyond the TF relation, we begin by plotting the K-band TF relation for our sample (Figure 1). One might expect evolution of the TF relation in the K-band to display a clearer signal than the B-band since the effects of dust are mitigated and passive evolution should be more uniform in its effect across the sample. When we assume that the slope of the K-band Tully-Fisher is the same as the local value from Verheijen (2001) we find no significant evolution, as is also found in the B-band (Vogt et al. 2005). We perform these fits using both a downhill simplex amoeba and Levenberg-Marquardt χ^2 minimization, both of which give the same results.

We find a fading of 0.04 ± 0.24 magnitudes for systems at $z > 0.7$ compared with the $z \sim 0$ relationship and a brightening of 0.37 ± 0.23 magnitudes for systems at $0.2 < z < 0.7$, consistent with no evolution. The scatter does not evolve significantly (1.13 magnitudes for the $z < 0.7$ sample, and 0.72 magnitudes for systems at $z > 0.7$). In all cases, the observed slope and scatter change only slightly when we ignore internal extinction corrections.

Although our results are broadly consistent with earlier, smaller samples, the interpretation of any evolutionary signal is complicated in two ways. First, only a limited range of luminosity and rotational velocity can be sampled at high redshift, leading to great uncertainties given the intrinsic scatter. Second, as luminosity and rotational ve-

larity are indirect measures of the assembly state of the galaxy, both may be evolving in complex ways, that mask actual evolutionary changes.

4.2. The Stellar Mass Tully-Fisher Relation

The first step beyond the TF relation is to compare the stellar mass to the measured maximum velocity - a relation we will call the *stellar mass - Tully Fisher relation*. The classical B-band TF relation scales such that $L \propto V^{3.5}$. This coupling becomes even steeper for the local stellar mass Tully-Fisher relation in nearby disks, $M \propto V^{4.5}$ (Bell & de Jong 2001).

Ideally, we seek to measure the all-inclusive baryonic TF relation, but measuring the gas content of high redshift disks is not yet feasible. We can estimate how much cold gas we are missing in our stellar mass inventory by investigating the gas mass fractions for nearby disk galaxies. Through examinations of the luminosities and HI masses for nearby disks, McGaugh & de Blok (1997) conclude that galaxies which are massive, bright, red, or have a high-surface brightness, have very little gas in comparison to bluer, fainter, lower surface brightness systems. Systems which are brighter than $M_B = -21$ have gas mass fractions that are typically 0.1 or lower. Since our selection finds the most luminous, high surface brightness systems, which are also red, they are the least likely sub-class of disks to have a high gas content.

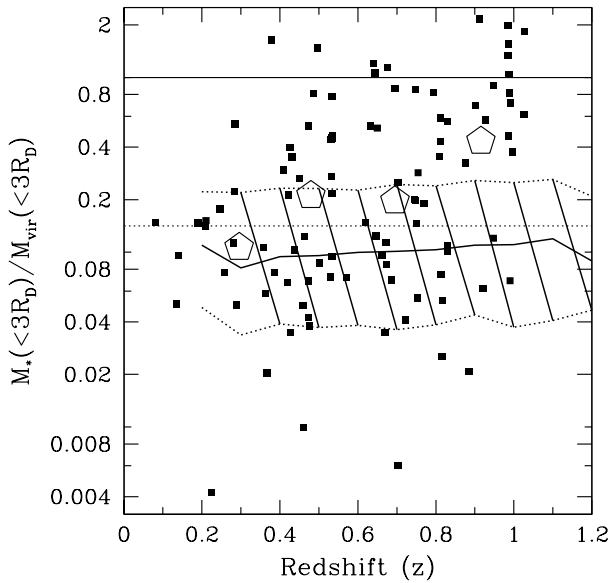


FIG. 3.— The relationship between the stellar mass and virial mass within $3R_d$ plotted as a function of redshift (z) for all galaxies in our sample. The pentagons show the average value of this ratio as a function of redshift. The solid horizontal line shows the location of $M_*(< R_d) / M_{\text{vir}}(< R_d) = 1$ while the horizontal dotted line is the universal baryonic mass limit. The solid line surrounded by the hatched region shows the predictions of a hierarchical Λ CDM based galaxy formation model (Baugh et al. 2004).

The stellar mass TF relation is shown in Figure 2 where, as before, we divide the sample into two redshift bins, split at $z = 0.7$. Each panel contains a solid line giving the $z \sim 0$ best fit and a dashed line illustrating the $\pm 3\sigma$ uncertainty in this fit (Bell & de Jong 2001). As was the case

for the conventional TF relations, no significant evolution in the zero-point is observed. The Bell & de Jong (2001) $z = 0$ stellar mass Tully-Fisher relation can be written as $M_* = 0.52 + 4.49 \times \log(V_{\text{max}})$. By holding the slope of this relationship constant, we find that the zero point is best fit by 0.45 ± 0.12 at $z < 0.7$ and 0.41 ± 0.13 at $z > 0.7$. Neither of these are however significantly different from the $z \sim 0$ relationship, and are very similar to each other. This implies that, if growth continues, the stellar and dark components are growing together. For example, if disk assembly since $z \simeq 0.7$ proceeded only by the addition of stellar mass at a uniform rate of $4 M_{\odot} \text{ year}^{-1}$, the local zero point would be discrepant at the 4σ level. This lack of evolution is important for understanding how disk galaxy formation is occurring (see §4.4).

Moreover, the scatter in the stellar mass Tully-Fisher relation is similar to that observed in the K-band Tully-Fisher after converting the K-band magnitude scatter into a luminosity and assuming an average stellar mass to light ratio. The typical scatter (in $\log M_*$ units) in stellar mass for these is 0.65 for disks at $z < 0.7$ and 0.48 for those at $z > 0.7$.

4.3. A Comparison of Stellar and Halo Masses

The final step in our analysis will be an attempt to convert our measured quantities into a comparison of the stellar and halo masses as discussed in §3. Recognizing the considerable uncertainties involved, Figure 3 shows as a function of redshift the ratio, $f_* = M_*/M_{\text{vir}}$, between the stellar masses and virial masses (eq. 1) within $3R_d$ for our sample. As expected, the stellar masses are nearly always less than the independently-derived virial masses, indicating that our methods for computing these values are not dominated by large systematic errors. It can also be seen from this figure that there is wide range of M_*/M_{vir} values at every redshift from $z \sim 0.2 - 1.2$. The open pentagons show the median values of f_* as a function of redshift. The dotted horizontal line shows the global baryonic mass fraction $\Omega_b/\Omega_m = 0.171$ derived from WMAP results (Spergel et al. 2003). Within $3R_d$ it appears that many disks have M_*/M_{vir} values higher than this limit. It also appears that within $3R_d$ the stellar mass of the disk dominates the virial mass. This indicates that within the visual parts of some of our sample, the disk component accounts for roughly all the mass, which is consistent with a maximal disk interpretation. However, there are clear examples on Figure 3 where either the stellar mass is overestimated and/or the virial mass is underestimated. Both of these are possibilities, since our stellar masses are potentially too high from using a Salpeter IMF, and we might be underestimating the value of V_{max} due to seeing, or a lack of depth in the LRIS observations. There is also a slight bias such that at higher redshifts nearly all galaxies sampled have high V_{max} values, which are likely maximal, while at lower redshifts we are sampling systems with lower V_{max} values, that have not yet fully formed their stellar masses. This is likely part of the reason that the stellar mass to virial mass ratio increases slightly at higher redshifts.

However, we are also interested in constraining the relationship between the total halo mass, M_{halo} , and the total stellar mass M_* . As we discuss in §3, it is very difficult to accurately obtain halo masses. We therefore show in

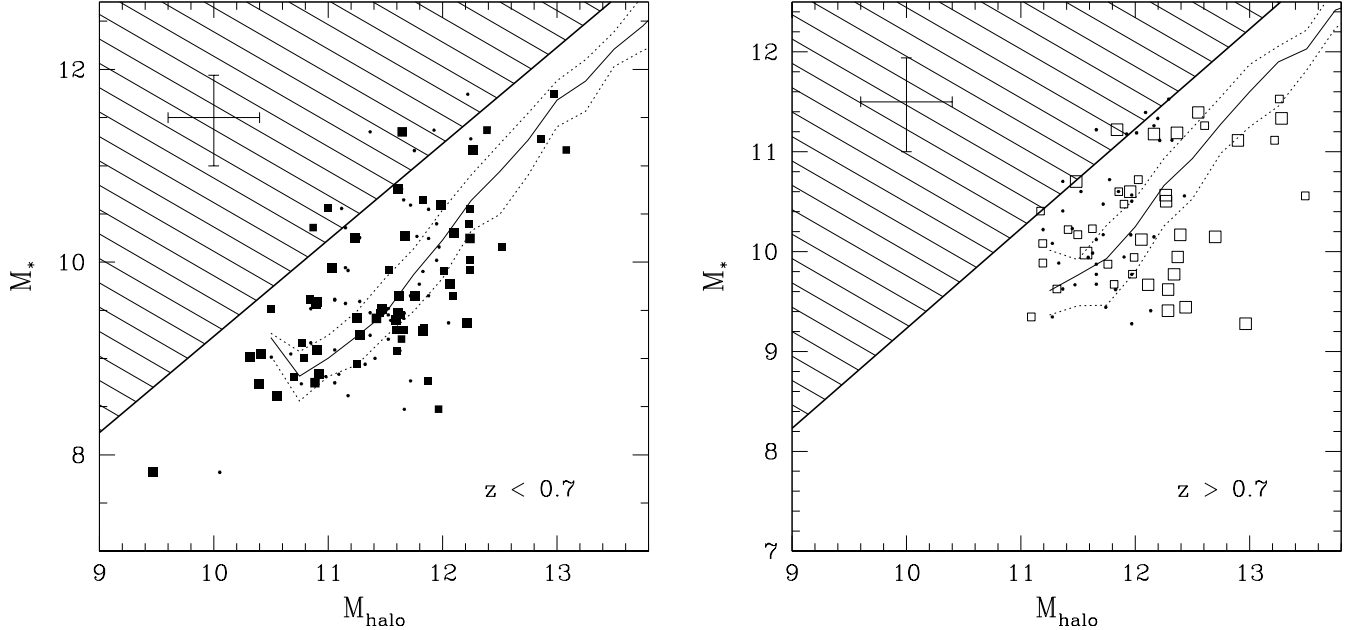


FIG. 4.— The relationship between stellar mass and halo masses in our two different redshift bins. The large symbols are for total masses derived from model relationships (eq. 2), and the small points are total halo masses derived using eq. (1) with $R = 100$ kpc. The thin solid line is the relationship between stellar and virial masses from the semi-analytic models of Benson et al. (2002) at $z = 0.4$ for the $z < 0.7$ sample and at $z = 0.8$ for the $z > 0.7$ sample. The short dashed lines display the 80% range of where galaxies in these simulation are found. The thick solid line is the baryonic fraction limit and the shaded region is the area where the stellar mass fraction is greater than the universal baryonic mass fraction.

Figure 4 total halo masses derived through eq. (1) at 100 kpc and through the semi-analytical approach (eq. 2). Although we cannot accurately determine total halo masses for individual systems, our main goal is to compare how the ratio of stellar to halo mass changes with redshift. Figure 4 shows this relationship divided into the same redshift bins as in Figures 1 & 2. To first order, the halo masses and stellar masses of disk galaxies should correlate if star formation is regulated in the same manner in halos of different masses (Steinmetz & Navarro 1999). Although there is no reason to expect any particular functional form between these two quantities, there is a reasonably well-fit linear relationship between them. We find that the zero point and slope of this relation does not change significantly between low and high redshift. There is also no obvious change in the scatter from high to low redshift (0.26 cf. 0.32). The most significant outcome of Figures 3 and 4 however is the remarkable similarity in trends found at high and low redshift suggesting some disks had completed the bulk of their stellar assembly by $z \simeq 1$ or more likely that the stellar and dark masses of galaxies grow together continuously.

Figure 5 shows the distribution of $f_* = M_*/M_{\text{halo}}$ for systems more massive than, and less massive than, the average halo mass, $M_{\text{halo}} = 10^{11.8} M_{\odot}$. The solid line is the universal baryonic mass ratio. As mentioned earlier, most disk stellar mass fractions are lower than the cosmic ratio, which seems appropriate given our stellar mass inventory is not intended to account for all associated baryons. Although some dispersion is expected, conceivably some fractions are overestimated or underestimated, for example by making incorrect assumptions about the IMF, or

underestimating V_{max} (and hence M_{halo}) by insufficient sampling of the rotation curve.

Figure 5 also shows a tentative population of disk galaxies with remarkably low stellar fractions, the most extreme cases occurring in objects with halo masses $M_{\text{vir}} > 10^{11.8} M_{\odot}$. These galaxies deviate from the $z = 0$ stellar mass TF relation by more than 4σ . Investigation of the individual systems that lie in this category shows them to be undergoing vigorous star formation as inferred by bluer than average ($U - B$) colors. A weak correlation was found between f_* and $(U - B)$. Because these systems are blue, they may have kinematic asymmetries in their rotation curves which may raise their V_{max} values. However, this is unlikely the effect producing this slight correlation as most of the low f_* systems also have low V_{max} values. We investigated several other possible correlations involving f_* (for example with the bulge/disk ratio) but no significant trends were found.

4.4. Comparison with Models

To investigate the implications of our results for the assembly history of stellar mass in disk galaxies since $z \sim 1$, we return to the behavior of the stellar fraction $f_* = M_*(<3R_d)/M_{\text{vir}}(<3R_d)$ vs. redshift (Figure 3), and the relationship between total stellar mass (M_*) and halo mass (M_{halo}) at $z > 0.7$ and $z < 0.7$ (Figure 4). Trends in these relations may shed light on the physical processes regulating star formation in disk galaxies. This is only the case however if the value of R_d for disks does not grow with time, which appears to be the case for the largest disks, based on our own limited data, and in statistical studies of $z > 0.8$ disks (Ravindranath et al. 2004; Conselice et

al. 2004; cf. Ferguson et al. 2004 for higher redshifts).

First, Figure 3 shows that the median stellar vs. virial mass value for our sample does not change significantly with redshift. We can compare two simple extreme models to this result to determine the likely method by which disk galaxies are forming at $z < 1$. In a ‘monolithic collapse’ model, where the dark halo and baryons for a galaxy are in place at high redshift, and there is no change in these mass components with time (e.g., Eggen, Lynden-Bell & Sandage 1962), the average value of M_*/M_{vir} should increase with time. This assumes that effective radii distribution for disks does not change with time, which is observed (Ravindranath et al. 2004). There is evolution in the monolithic model only in the sense that baryons are gradually converted to stars over time. This is the opposite to the observed trend in which the ratio of M_*/M_{vir} is roughly constant.

On the other hand, in a hierarchical picture, the value of M_*/M_{vir} remains relatively constant with time. Shown in Figure 3 are model predictions from *Galform* which show that the value of M_*/M_{vir} remains relatively constant with redshift. While we do not have a complete sample, we do find that the average and median values of M_*/M_{vir} for our sample remain constant with redshift within the errors, which is consistent with the hierarchical idea. The higher average M_*/M_{vir} value at $z > 0.8$ is likely produced by our selection of the brightest disks at these redshifts (Vogt et al. 2005). The *Galform* model however does not predict the full range of mass fractions that we find. At all redshifts there are systems dominated within R_d by their stellar masses, while some systems have low M_*/M_{vir} ratios. This is either produced by an observational bias (§4.3), or the simulations predict too much dark matter in the centers of disks.

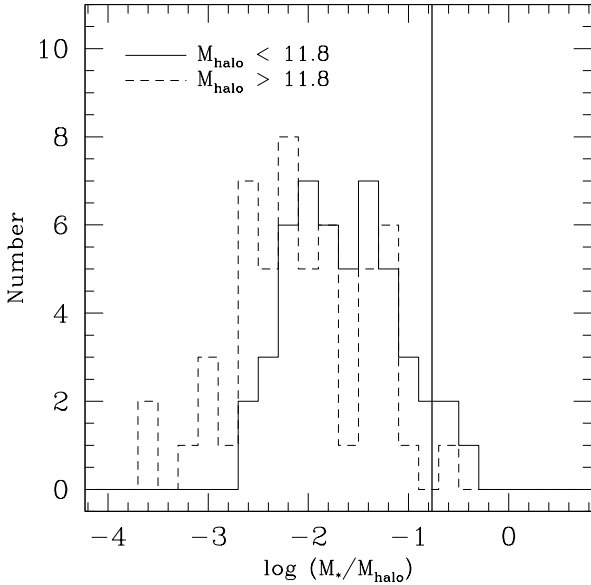


FIG. 5.— Histogram of M_*/M_{halo} values divided into disks of different virial masses. The solid line is the global baryonic mass fraction.

Figure 4 shows the relationship between total stellar and total halo masses (see §3.1) for our sample, divided into our

two redshift ranges. We also show on Figure 4 the *Galform* semi-analytic model values for this relationship for disk dominated galaxies with the 80% completeness indicated. As in Figure 3, no strong evolution in M_*/M_{halo} ratios is predicted. As galaxies in the semi-analytic models grow by accreting smaller systems, or intergalactic gas coupled with dark matter, and then converting the newly-obtained gas into stars quickly, the relationship between M_* and M_{halo} remains constant. This is generally what we find, as well as a good agreement with the model predictions. In fact, the agreement between the total stellar and halo masses with the *Galform* models is slightly better than the comparison between the stellar and virial masses with $3 \times R_d$, which further suggests that the luminous components of disk galaxies are dominated by the stellar mass (§4.3).

In summary, the fact that the ratio M_*/M_{halo} remains relatively constant in our sample with redshift, and that the stellar-mass TF relation does not evolution, are indications that disk galaxies are forming through the accretion of both dark and baryonic mass. Disk galaxies are undergoing star formation at $z < 1$ at a rate of a few solar masses per year. If disks at $z \sim 1$ contained all the baryonic or halo masses that they have at $z \sim 0$, we would see an increase in M_*/M_{halo} with time. Because we do not see this trend, it appears that new stars form out of gas accreted from the intergalactic medium, which is coupled with dark matter at a constant ratio. This baryonic to dark matter ratio is such that both M_* and M_{halo} grow with time, creating a stellar mass to halo mass ratio that is on average relatively constant.

5. CONCLUSIONS

We present the results of a dynamical and structure study of 101 disk galaxies drawn mostly from the DEEP1 survey with redshifts in the range $z \simeq 0.2-1.2$. New infrared imaging observations are presented which enable us to derive reasonably reliable stellar masses and thereby to construct the stellar mass Tully-Fisher relation and its redshift dependence. Using various formalisms drawn from analytic and semi-analytical models, we attempt to convert our dynamical data to make the first comparisons of the relative fractions of stellar and total mass in our sample. Notwithstanding the considerable uncertainties and sample incompleteness, the results are encouraging and suggest remarkably little evolution in the mix of baryons and dark matter since $z \simeq 1$.

Although our sample is not formally complete in luminosity or mass, we explore the degree to which there may have been evolution in the relative distribution of stellar and virial masses and find the following:

1. Massive disk galaxies exist out to $z \sim 1$ with halo masses as large as $10^{13} M_{\odot}$, roughly as large as the most massive disks in the nearby universe. These systems also contain a large amount of stellar mass. At least some disk galaxies are nearly fully mature in their stellar content at $z \sim 1$.
2. We confirm earlier studies based on smaller samples and find no significant evolution in the zero point or scatter of the rest-frame K -band Tully-Fisher relation out to $z \sim 1.2$.

3. The stellar mass Tully-Fisher relation out to $z \sim 1.2$ is likewise largely consistent with the relation found for nearby disks. We find no significant evolution in our sample after comparing systems at redshifts greater than and less than $z = 0.7$.
4. Although there are clearly great uncertainties in estimating total halo masses from our dynamical data, we find the distribution of the ratio of stellar and halo masses remains relatively similar from $z \sim 0$ to $z \sim 1.2$. The stellar fraction observed can be understood if the bulk of the baryons associated with massive disk galaxies have already formed their stars. A modest number of massive galaxies have very low stellar fractions, consistent with continued star formation as revealed by their blue $U - B$ colors.
5. These results are in relatively good agreement with Λ CDM analytical and semi-analytical models (Benson et al. 2002; Baugh et al. 2005), suggesting that disk galaxy formation is hierarchical in nature.

Our overarching conclusion from this study is that no significant evolution in the stellar mass fraction can be detected in the population of regular massive disks since $z \simeq 1$. Although biases and uncertain assumptions may affect detailed quantities at the 0.3 – 0.5 dex level, the absence of gross trends is consistent with the conclusion that the bulk of these systems grow at $z < 1$ by the accretion of dark and baryonic material. This conclusion is

however tempered by the fact that our selection is affected by a bias that likely changes with redshift. For example, because our sample was selected by a $I < 23$ limit, we are studying the brightest disks at the highest redshifts.

These results, while intriguing, will be examined in much greater detail with the upcoming DEEP2 redshift survey (Davis et al. 2002), which will combine near-infrared imaging from the Hale 5 meter telescope with rotation curves obtained using the DEIMOS spectrograph on the Keck II telescope. There are several issues that can be better addressed with deeper spectroscopy and a more careful selection of high- z disks. The total number of disks in this much larger sample is expected to be on the order of thousands and will solidify and expand on the preliminary results revealed by this study.

We thank the DEEP team for generously enabling us to augment their optical sample and catalogs with near-infrared data in order to make this comparison. We also thank Cedric Lacey and Andrew Benson for access to their semi-analytical model simulation results, and Xavier Hernandez and Ken Freeman for comments regarding this work. CJC acknowledges support from a National Science Foundation Astronomy and Astrophysics Postdoctoral Fellowship. NPV is pleased to acknowledge support from NSF grants NSF-0349155 from the Career Awards program, NSF-0123690 via the Advance IT program at NMSU, and AST 95-29098 and 00-71198 administered at UCSC, and NASA STScI grants GO-07883.01-96A, AR-05801.01, AR-06402.01, and AR-07532.01.

REFERENCES

Abadi, M.G., Navarro, J.F., Steinmetz, M., & Eke, V.R. 2003, ApJ, 591, 499

Baugh, C.M., Lacey, C.G., Frenk, C.S., Granato, G.L., Silva, L., Bressan, A., Benson, A.J., & Cole, S. 2005, MNRAS, 356, 1191

Bell, E.F., & de Jong, R.S. 2001, ApJ, 550, 212

Benson, A.J., Cole, S., Frenk, C.S., Baugh, C.M., & Lacey, C.G. 2000, MNRAS, 311, 793

Benson, A.J., Lacey, C.G., Baugh, C.M., Cole, S., & Frenk, C.S. 2002, MNRAS, 333, 156

Bohm, A., et al. 2004, A&A, 420, 97

Brinchmann, J., & Ellis, R.S. 2000, ApJ, 536, L77

Brinchmann, J., et al. 1998, ApJ, 499, 112

Brinchmann, J. 1999, PhD, Cambridge University

Bruzual, A.G., & Charlot, S. 2003, MNRAS, 344, 1000

Bundy, K., Fukugita, M., Ellis, R.S., Kodama, T., & Conselice, C.J. 2004, ApJ, 601, L123

Bundy, K., Ellis, R.S., & Conselice, C.J. 2005, ApJ, astro-ph/0502204

Calzetti, D. 1997, AJ, 113, 162

Cole, S., Lacey, C.G., Baugh, C.M., & Frenk, C.S. 2000, MNRAS, 319, 168

Charlot, S., Worthey, G., & Bressan, A. 1996, ApJ, 457, 625

Conselice, C.J. et al. 2004, ApJ, 600, L139

Davis, M., et al. 2002, SPIE, 4834, 161

de Jong, R.S. 1996, A&A, 118, 557

Dickinson, M., Papovich, C., Ferguson, H. C., & Budávari, T. 2003, ApJ, 587, 25

Drory, N., Bender, R., Feulner, G., Hopp, U., Maraston, C., Snigula, J., & Hill, G.J. 2004, ApJ, 608, 742

Eggen, O.J., Lynden-Bell, D., & Sandage, A.R. 1962, ApJ, 136, 748

Gronwall, C., & Koo, D.C. 1995, ApJ, 440, L1

Groth, E.J., Kristian, J.A., Lynds, R., O'Neil, E.J., Balsano, R., Rhodes, J. 1994, BASS, 185, 5309

Ferguson, H.C., et al. 2004, ApJ, 600, L107

Haynes, M.P., et al. 1999, AJ, 117, 2039

Kauffmann, G., et al. 2003, MNRAS, 341, 33

Kinney, A., Calzetti, D., Bohlin, R., McQuade, K., Storchi-Bergmann, T., & Schmitt, H.R. 1996, ApJ, 467, 38

Madau, P., Pozzetti, L., & Dickinson, M. 1998, ApJ, 498, 106

McGaugh, S.S., & de Blok, W.J.G. 1997, ApJ, 481, 689

Matthews, K., & Soifer, B.T. 1994, in "Infrared Astronomy with Arrays, The Next Generation", edited by Ian S. McLean, 190, 239

Motohara, K., et al. 2002, PASJ, 54, 315

Oke, J.B. et al. 1995, PASP, 107, 375

Papovich, C., Dickinson, M., & Ferguson, H.C. 2001, ApJ, 559, 620

Peng, C.Y., Ho, L.C., Impey, C.D., & Rix, H-W. 2002, AJ, 124, 266

Persic, M., & Salucci, P. 1991, ApJ, 368, 60

Poggianti, B.M. 1997, A&AS, 122, 399

Poggianti, B.M., & Barbaro, G., 1996, A&A, 314, 379

Ravindranath, S., et al. 2004, ApJ, 604, L9

Roche, P.F. 2003, SPIE, 4841, 901

Schlegel, D.J., Finkbeiner, D., & Davis, M. 1998, ApJ, 500, 525

Simard, L. et al. 2002, ApJS, 142, 1

Sofue, Y., & Rubin, V. 2001, ARA&A, 39, 137

Spergel, D.N. et al. 2003, ApJS, 148, 175

Steinmetz, M., & Navarro, J.F. 1999, ApJ, 513, 555

Tully, R.B., & Fisher, J.R. 1977, A&A, 54, 661

Tully, R.B., Pierce, M.J., Huang, J.-S., Saunders, W., Verheijen, M.A.W., & Witchalls, P.L. 1998, AJ, 115, 2264

van den Bosch, F.C. 2002, MNRAS, 332, 456

Verheijen, M.A.W. 2001, ApJ, 563, 694

Vogt, N.P., Forbes, D.A., Phillips, A.C., Gronwall, C., Faber, S.M., Illingworth, G.D., & Koo, D.C. 1996, ApJ, 465, L15

Vogt, N.P., et al. 1997, ApJ, 479, L121

Vogt, N.P., et al. 2004, ApJ, submitted

Vogt, N.P., et al. 2005, in preparation

Weiner, B.J., et al. 2004, ApJ, in press

Williams, R., et al. 1996, AJ, 112, 1335

White, R.E., III., Keel, W.C., Conselice, C.J. 2000, ApJ, 542, 761

Wilson, J.C., et al. 2003, SPIE, 4841, 451

Ziegler, B.L. et al. 2002, ApJ, 564, L69